Chapter -3

Soft Chemical Synthesis, Magnetic and Microwave Studies of $CuFe_2O_4$ and $CoFe_2O_4$

✶ **A part of this work has been published:**

T. George, S. Joseph, S. Mathew, *J. Metastable and Nanocryst. Mater.* 23 (2005) 141

✶ **A part of this work has been presented:**

1. T. George, S. Joseph, S. Mathew, *International Conference on Materials for Advanced Technologies, ICMAT-2003*, NUS, Singapore, 7-12 December, 2003
2. T. George, S. Joseph, A.T. Sunny, S. Mathew, *National Review and Coordination Meeting on Nanoscience and Nanotechnology, NS & NT 2007*, Hyderabad, 21-23 February, 2007

3.1. Introduction

The nanoparticles obtained usually have a strong tendency to aggregate, which makes it very difficult to exploit their unique physical properties. Dispersion of the nanoparticles in a matrix is one method for reducing particle agglomeration and this method allows one to stabilize the particles. In most cases, the synthesized particles are poorly crystalline and calcination at high temperature is needed to induce the high crystalline structures [1] and magnetic hardening occurs after heat treatment at a relatively high temperature [2]. The sol-gel method is one of the soft chemical routes for the preparation of nanosized particles. This synthetic method has several advantages like good stoichiometric control, atomic level mixing and short processing time at low temperatures. For then synthesis of nanomaterials, poly acrylic acid (PAA) can be used as the chelating agent and it can also act as a matrix [3]. The use of polyacrylic acid as a chelating agent has got the advantage of reducing the calcination temperature since the heat of combustion of PAA is utilized for the crystallization of the particles. Compared with citric acid, the conventional chelating agent, PAA has more carboxylic groups to form chelates with mixed cations and results in a sol. It also greatly aids in the formation of a cross-linked gel, which may provide more homogenous mixing of cations and less tendency for aggregation during calcinations. The usual ceramic method of preparing ferrispinels requires high calcinations temperature resulting in inhomogeneous and aggregate particles with low surface areas.

3.2 Experimental

We have synthesized copper ferrite and cobalt ferrite nanoparticles by sol-gel method using PAA as the chelating agent, and investigated its microwave dielectric and magnetic properties [4]. Copper nitrate and ferric nitrate were used as the precursors. All the chemicals were supplied by Merck. Nitrate precursors were used because of their easy solubility in water. The synthesized ferrite powders were characterized using XRD, EDAX FE-SEM, and SEM. The room temperature magnetic properties of the synthesized ferrite powders were determined using vibrating sample magnetometer (VSM). The microwave dielectric parameters such as real and imaginary part of complex permittivity, loss tangent and a.c. conductivity were evaluated using a transmission type S-band rectangular cavity resonator with a dimension of [35.3 x 7.2 x 3.35 cm^3] and a network analyzer.

3.2.1. Synthesis and characterization of $CuFe_2O_4$ nanoparticles

Required amount of PAA was synthesized by the free radical polymerization of acrylic acid [5]. Copper nitrate (0.4M) and ferric nitrate (0.8M) solutions were mixed with aqueous solution of PAA. The molar ratio of the amount of PAA to total metal ions was taken to be 2:1. Phase separation was observed. With constant stirring, an appropriate amount of nitric acid was slowly added to this solution until a transparent green solution (pH 1-3) was obtained. The resulting solution was evaporated at 50°C until a transparent sol was formed. Then, the transparent sol was heated at 50°C for10 hours to remove water. The sol turned into a viscous greenish-blue gel. The gels were prepared with different molar ratios of PAA to the total metal ions. The gel on calcination at 400°C for 2 hours at a heating rate of 5°Cmin^{-1} yields brown-black coloured $CuFe_2O_4$ nanoparticles.

X-ray powder diffraction patterns were recorded using Rigaku D/MAX X-ray diffractometer with Cu K_α radiation (λ = 0.1542 nm). The surface morphology and homogeneity were studied using a scanning electron microscope, SEM (JEOL model No. JSM-5600LV) and a field emission scanning electron microscope, FE-SEM (NOVA NANOSEM 600 FEI). Thermogravimetric analysis and differential thermal analysis (TGA and DTA) of the gels were carried out in nitrogen atmosphere from the temperature range, room temperature to 500 °C using Schimadzu DTG 60.

3.2.2. Synthesis and characterization of $CoFe_2O_4$ nanoparticles

All the reagents used were A.R. grade without further purification. A mixture of 6 ml. each of cobalt nitrate (0.4 M) and ferric nitrate (0.8 M) solutions were added to an aqueous solution of PAA. The molar ratio of the amount of PAA to total metal ions was taken to be 2:1 for the sample. Phase separation was observed. With constant stirring, an appropriate amount of nitric acid was slowly added to this solution until a transparent pink solution (pH = 1-3) was obtained. The resulting solution was evaporated at 50 °C until a transparent sol was formed. Then, the transparent sol was heated at 50 °C for 10 hours to remove water. The sol turned into a viscous pink gel. The gel on calcination at 450 °C for 3 hours at a heating rate of 5 °C min^{-1} in a programmable muffle furnace yielded 0.75 g brown colored $CoFe_2O_4$ nanoparticles.

The phase structure characterization of the synthesized powder were carried out by powder X-Ray diffraction (XRD) using PANalytical X'Pert PRO diffractometer with Cu K_α radiation (λ = 0.1542 nm). Studies on the surface morphology, homogeneity and energy-dispersive X-ray analysis (EDX) of the powders were carried out using a scanning electron microscope

SEM (JEOL model No. JSM-5600LV) and a field emission scanning electron microscope, (NOVA NANOSEM 600 FEI). Thermogravimetric analysis (TGA) and differential thermal analysis (DTA) of the gels were carried out in nitrogen atmosphere from the temperature range, room temperature to 500 °C using Schimadzu DTG 60.

3.2.3. Investigation of magnetic properties of $CuFe_2O_4$ and $CoFe_2O_4$

The magnetic properties of the synthesized nanoparticles were measured using a vibrating sample magnetometer (VSM-Lakeshore) at room temperature and the hysteresis loop was drawn with the magnetic field, cycled between –10000 to 10000 G.

3.2.4. Investigation of microwave dielectric properties of $CuFe_2O_4$ and $CoFe_2O_4$

A part of the synthesized ferrite powders were mixed with PVA and pressed at 5 ton $inch^{-2}$ to form a pellet of thickness 1.7 mm and diameter 10 mm. The pellet was calcined at 500 °C for two hours to remove PVA. The experimental set up for the determination of microwave dielectric properties consists of a transmission type S-band rectangular cavity resonator and a network analyzer [6-8]. The rectangular cavity is connected to the Agilent 8714 ET network analyzer (frequency range 300 KHz - 3GHz). The sample in the form of pellet was loaded into the resonant cavity excited in the dominant transverse electric (TE) mode. Each cavity has a series of characteristic resonant frequencies. When a sample was placed inside the cavity it will affect the resonant frequencies and the Q values. Resonant frequencies and the corresponding Q values of the sample loaded cavity and of the air filled cavity were measured. The microwave dielectric parameters such as real and

imaginary part of complex permittivity, loss tangent and a.c. conductivity were evaluated. The theory was explained elsewhere [7-9].

3.2.5. Investigation of microwave magnetic properties of $CuFe_2O_4$ and $CoFe_2O_4$

To find the complex permeability, the sample powders were tightly filled in thin capillary tubes of low loss material and sealed. Each tube was then inserted through the non-radiating slot on the broad wall of the wave-guide cavity, and held with a thin sample holder made of low loss material. Resonant frequencies and the corresponding Q values of the sample loaded cavity and of the air filled cavity were measured in the TE mode. Then the magnetic parameters such as the real and imaginary part of complex permeability (Table 2.4 and 2.5) were evaluated according to the theory explained elsewhere [8, 10, 11].

3.3. Results and discussion

3.3.1. Powder XRD study of $CuFe_2O_4$ and $CoFe_2O_4$

Figure 3.1 shows the powder XRD pattern of the synthesized copper ferrite nanoparticles. All the peaks in the pattern are indexed to the pure cubic phase (JCPDS Card No 77-0010) of $CuFe_2O_4$ with space group Fd3m and lattice parameter, a = 8.373 Å.

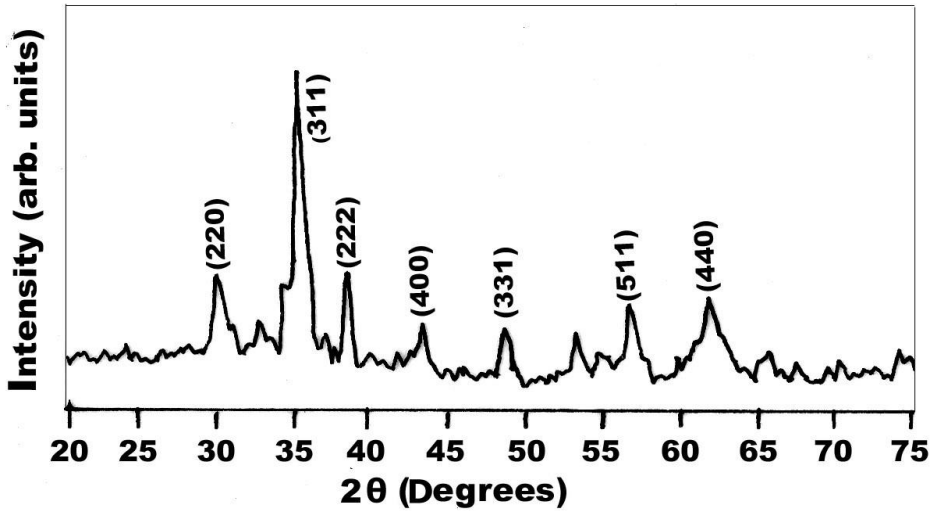

Figure 3.1. XRD pattern of synthesized $CuFe_2O_4$ nanoparticles.

The average crystallite size estimated using the Scherrer equation is 12 nm. It can be noticed that the diffraction peaks are broadened and can be attributed to the reduction in the particle size of the synthesized $CuFe_2O_4$ nanoparticles.

Figure 3.2 shows the powder XRD pattern of the synthesized cobalt ferrite nanoparticles. All diffraction peaks are indexed to a pure cubic phase (JCPDS Card No 22-1086) of $CoFe_2O_4$ with space group Fd3m. The estimated lattice parameter, a = 8.388 Å well agrees with the JCPDS file. The average crystallite size estimated using the Scherrer equation [12] for $CoFe_2O_4$ is 18 nm.

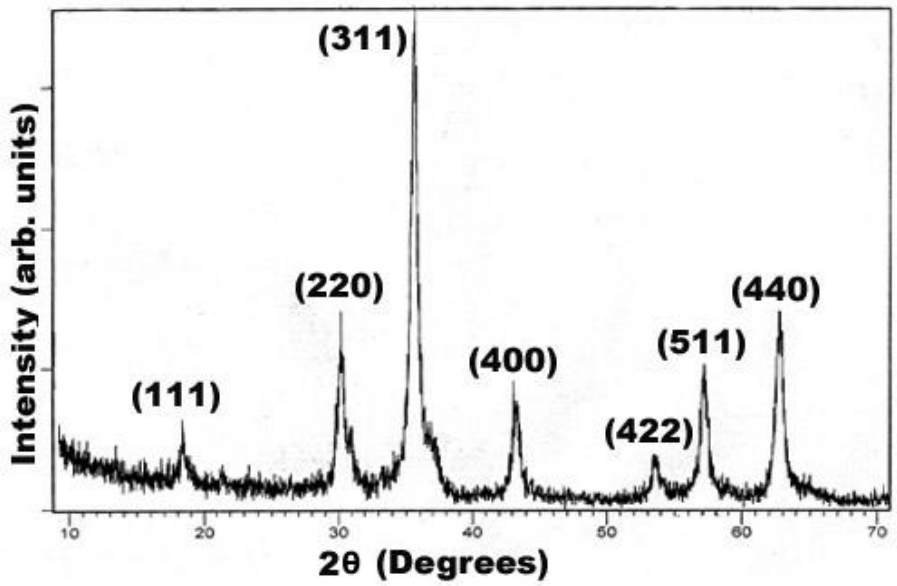

Figure 3.2. XRD pattern of synthesized $CoFe_2O_4$ nanoparticles.

All the diffraction peaks exactly matches with the JCPDS data showing the phase purity the synthesized $CuFe_2O_4$ and $CoFe_2O_4$ nanoparticles. The broadened diffraction peaks can be attributed to the reduced particle size of the synthesized products**.**

3.3.2.Thermal analysis of $CuFe_2O_4$ and $CoFe_2O_4$ gels

Figures 3.3 and 3.4 show the recorded thermal gravimetric (TG) and differential thermal analysis (DTA) curves of the evaporated dry gel in nitrogen atmosphere at a heating rate of 5 ˚C min^{-1}.

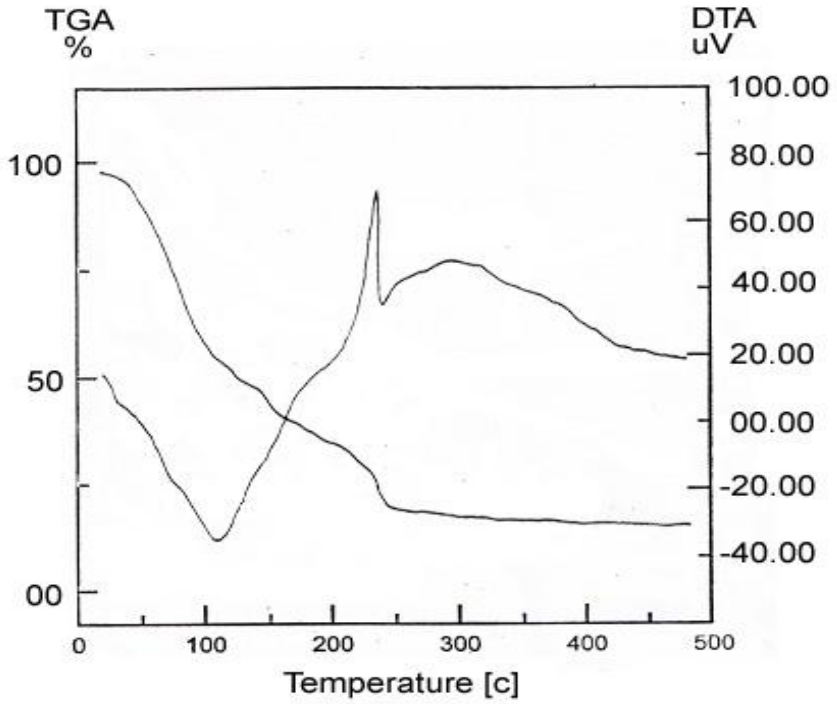

Figure 3.3. TGA-DTA curves of copper ferrite gel before calcination

The thermograms of both $CuFe_2O_4$ and $CoFe_2O_4$ gels look almost identical. The DTA curve shows an endothermic peak around 100˚C due to the drying of the gel. The TGA curve also shows the corresponding weight loss up to 250˚C due to the drying and decomposition of the gel. Above 250 ˚C there is no considerable weight loss in the TGA curve.

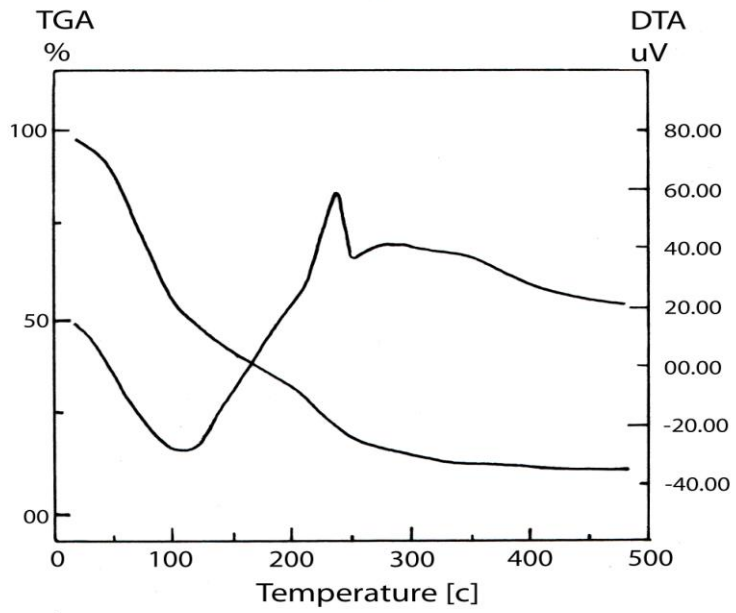

Figure 3.4. TGA-DTA curves of cobalt ferrite gel before calcination

The exothermic peak around 250°C in the DTA curve is assumed to be due to the crystallization of ferrite from the gel. The broad exothermic peak around 300°C is due to the combustion of PAA.

3.3.3. Electron microscopic studies of $CuFe_2O_4$ and $CoFe_2O_4$

3.3.3.1. FE-SEM analysis

Figure 3.5 (a) and (b) shows the FE-SEM images of the $CuFe_2O_4$ and $CoFe_2O_4$ nanoparticles. It can be seen that the particles are almost spherically shaped and uniformly arranged. The particle size estimated from the FE-SEM analysis agrees well with the XRD results.

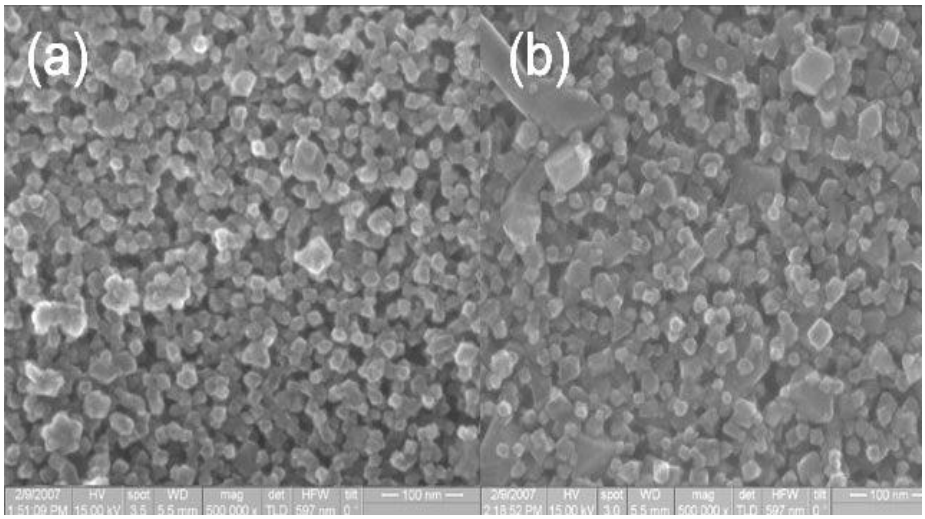

Figure 3. 5. FE-SEM image of **(a)** $CuFe_2O_4$ **(b)** $CoFe_2O_4$ nanoparticles.

The EDX analysis in figure 3.6 (a) and figure 3.6 (b) respectively shows the co-existence of Cu, Fe and oxygen consistent with $CuFe_2O_4$ composition and Co, Fe and oxygen consistent with $CoFe_2O_4$ composition.

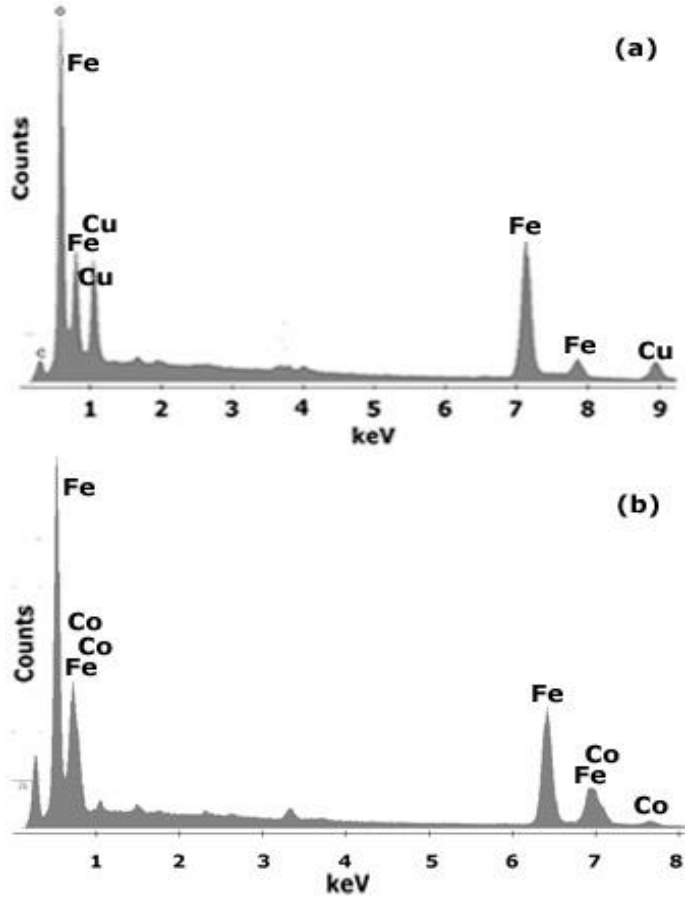

Figure 3.6. EDX spectra of **(a)** $CuFe_2O_4$ **(b)** $CoFe_2O_4$ nanoparticles.

3.3.3.2. SEM analysis

The scanning electron microscopic (SEM) images of $CuFe_2O_4$ and $CoFe2O_4$ are shown in figure 3.7 (a) and figure 3.7 (b). The agglomeration of the crystallites is prevented since the precursors got trapped in the nanosized net-like structure and channels of the gel formed by PAA. Further, the heat of

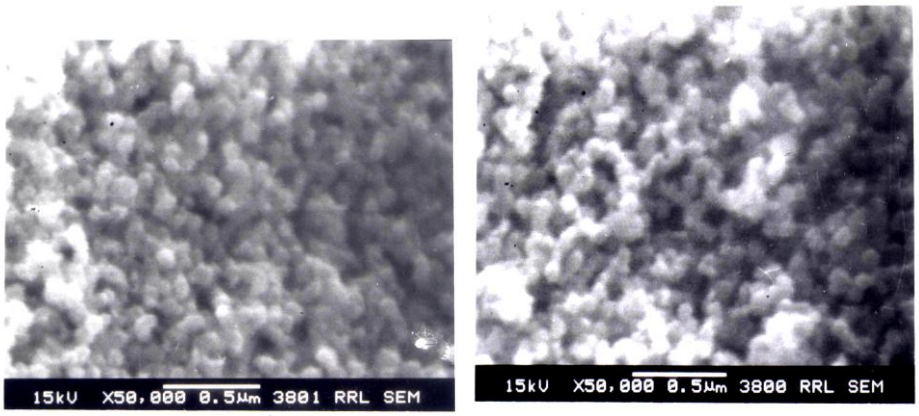

Figure 3.7. SEM photographs of (a) $CuFe_2O_4$ and (b) $CoFe_2O_4$ nanoparticles calcined at 400°C

combustion of PAA augmented the crystallization of the ferrites. The SEM photographs show that the particles are nearly monodispersed and approximately spherical.

3.3.4. Material studies of $CuFe_2O_4$ and $CoFe_2O_4$

3.3.4. 1. Magnetic property by VSM study

Figure 3.8 (a) and figure 3.8 (b) show the hysteresis curves of $CuFe_2O_4$ and $CoFe_2O_4$ nanoparticles. At room temperature, the samples exhibited hysteresis loop typical of magnetic behaviors indicting the presence of an ordered magnetic structure. The satuaration magnetization (Ms) value calculated for $CuFe_2O_4$ and $CoFe_2O_4$ nanoparticles are 15 emu/g and 30 emu/g which is also lower than the reported value for the bulk (55 and 80 emu/g) [13]. The decrease in the density of magnetization of the nanoparticles with respect to the bulk can be attributed to surface defects and morphology. The surface defects are the results of finite-size scaling of nanocrystallites, which in turn leads to a non-collinearity of magnetic moments on their surface.

These effects are more intense in ferromagnetic system, where the super-exchange interaction occurs through the oxygen ion, O^{2-} [14]. The coercivity recorded is approximately 300 G for $CuFe_2O_4$ and 1100 G for $CoFe_2O_4$ nanoparticles.

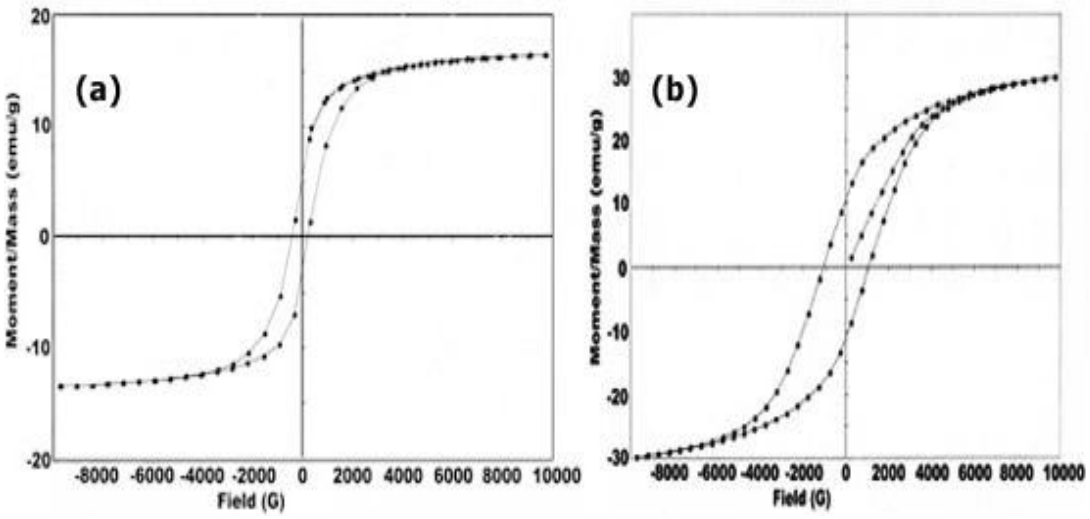

Figure 3.8. Hysteresis curves of **(a)** $CuFe_2O_4$ **(b)** $CoFe_2O_4$ nanoparticles

The average crystallite size of $CoFe_2O_4$ nanoparticles is higher compared to $CuFe_2O_4$ nanoparticles. The increase in magnetization and coercivity of $CoFe_2O_4$ is due to the increase in the crystallite size. Very small changes in particle size can lead to large changes in coercivity. These magnetization curves demonstrate that the as-prepared $CuFe_2O_4$ nanoparticles at room temperature tends to be more superparamagnetic compared to $CoFe_2O_4$, as the field is cycled between –10000 and 10000 G. The superparamagnetic behavior should be attributed to the extremely fine

crystallite size and regular shape of the material [15], which makes it easier for them to be thermally activated to overcome the magnetic anisotropy.

The extremely fine crystallite size and regular shape of the materials are evident from the FE–SEM studies. Generally, when the size of magnetic materials is smaller than the superparamagnetic critical dimension, above the blocking temperature its thermal fluctuation can overcome anisotropy, so the moments can rotate among the different easy directions and superparamagnetism is exhibited [16].

3.3.4.2. Microwave dielectric properties of $CuFe_2O_4$ and $CoFe_2O_4$

The material losses in the ferrite, like dielectric losses and magnetic losses may be represented by giving complex values to permittivity and permeability. Microwave dielectric parameters of $CuFe_2O_4$ nanoparticles (sample density =$2.4x10^3$ kgm^{-3}) and $CoFe_2O_4$ (sample density=$2.5x10^3$ kgm^{-3}) at various resonant frequencies are given in the following tables (tables 3.1-3.4).

Table 3.1. Variation of real part of complex permittivity ε_r' with frequency

Frequency (MHz)	**Real part of complex permittivity ε_r'**	
	$CuFe_2O_4$	**$CoFe_2O_4$**
2247.999	3.7810	7.9040
2440.356	3.8820	7.8030
2685.257	3.8110	7.7200
2971.572	3.8020	7.6510

The real part of complex permittivity ε_r' (table 3.1) of both the samples (density = $2.4x10^3 kgm^{-3}$ and $2.5x10^3$ kgm^{-3}) shows almost constant values over

the frequency range 2248- 2971 MHz. Imaginary part of complex permittivity ε_r'' (table 3.2) and the loss tangent (table 3.3) decreases slightly. The Imaginary part of complex permittivity component is responsible for the total loss of energy in the dielectric and tan δ is a measure of it [17].

Table 3.2. Variation of imaginary part of complex permittivity ε_r'' with frequency

Frequency (MHz)	**Imaginary part of complex permittivity ε_r''**	
	$CuFe_2O_4$	**$CoFe_2O_4$**
2247.999	0.1480	0.3120
2440.356	0.1420	0.2920
2685.257	0.1410	0.2660
2971.572	0.1350	0.2450

Table 3.3. Variation of Tan δ (loss tangent) with frequency

Frequency (MHz)	**Tan $\delta = \varepsilon_r''/\varepsilon_r'$**	
	$CuFe_2O_4$	**$CoFe_2O_4$**
2247.999	0.0390	0.0396
2440.356	0.0366	0.0374
2685.257	0.0369	0.0345
2971.572	0.0356	0.0320

The electric polarization makes a phase difference δ with the electric displacement. The a.c. conductivity σ_e (table 3.4) is found to be increasing as the frequency increases.

Table 3.4. Variation of a.c. conductivity with frequency

Frequency (MHz)	**a.c. conductivity (Sm^{-1})**	
	$CuFe_2O_4$	**$CoFe_2O_4$**
2247.999	0.018475	0.038981
2440.356	0.019194	0.039604
2685.257	0.020950	0.039698
2971.572	0.022296	0.040462

The variation of a.c. conductivity is explained on the basis of small polaron hopping mechanism [18-21]. The electron hopping occurs by electron transfer between adjacent octahedral sites in the spinel lattice [22, 23]. The a.c. conductivity and the Tan δ values of $CoFe_2O_4$ nanoparticles are observed to be high compared to $CuFe_2O_4$ nanoparticles. This can be attributed to the high magnetic moment possessed by $CoFe_2O_4$.

3.3.4.3. Microwave magnetic properties

Magnetic parameters of $CuFe_2O_4$ nanoparticles (sample density = $0.45x10^3$ kgm^{-3}) and $CoFe_2O_4$ nanoparticles (sample density = $0.46x10^3$ kgm^{-3}) at various resonant frequencies are shown in tables 3.5-3.7.

The real part of complex permeability μ_r' (table 3.5) imaginary part of complex permeability μ_r''(table 3.6) and the corresponding loss tangent

(table 3.7) of $CuFe_2O_4$ nanoparticles and $CoFe_2O_4$ nanoparticles decrease continuously over the frequency range 2248-2971 MHz.

Table 3.5. Variation of real part of complex permeability μ_r' with frequency

Frequency (MHz)	**Real part of Complex permeability μ_r'**	
	$CuFe_2O_4$	**$CoFe_2O_4$**
2247.999	4.3770	8.3270
2440.356	3.1950	7.9410
2685.257	3.3060	7.6120
2971.572	2.8690	7.3080

Table 3.6. Variation of imaginary part of complex permeability μ_r'' with frequency

Frequency (MHz)	**Imaginary part of complex permeability μ_r''**	
	$CuFe_2O_4$	**$CoFe_2O_4$**
2247.999	0.1118	0.4162
2440.356	0.0931	0.3861
2685.257	0.0491	0.2923
2971.572	0.0204	0.2672

The loss tangent (magnetic) is calculated using the formula,

$$\text{Tan } \delta = \mu_r''/\mu_r'$$

The eddy current loss in a material can be expressed in terms of tan δ. It is known that ferrites possess feeble eddy currents, which agrees very well with the experimental results. The decrease in loss tangent is due to the fact

that, when the frequency of the field increases the dipoles cannot follow the rapid variation of the field.

Table 3.7. Variation of Tan δ with frequency

Frequency (MHz)	**Tan δ = μ_r''/μ_r'**	
	$CuFe_2O_4$	**$CoFe_2O_4$**
2247.999	0.0255	0.0500
2440.356	0.0291	0.0486
2685.257	0.0149	0.0384
2971.572	0.0071	0.0365

The values of permeability, permittivity and a.c. conductivity are not really constant for a given material but usually have a strong dependence on frequency [24]. As the conductivity of the material is increasing with frequency, (table 3.4) the internal impedance of the material can be assumed to be decreasing. Since the internal impedance is a function of permeability this decrease is justifiable (table 3.5). When the frequency increases the magnetic dipoles of the crystallites cannot follow the fast variation of the applied field. The result is similar to that obtained by U. Raveendranath et al. [10]. In his study D.H. Chen et al. has reported a decrease in the value of saturation magnetization, M_s of $NiFe_2O_4$ nanoparticles with respect to the bulk material. The decrease in M_s of $NiFe_2O_4$ nanoparticles was explained as superparamagnetic nature of the material [3]. The superparamagnetic nature of the $CuFe_2O_4$ and $CoFe_2O_4$ nanoparticles might have affected the experimental values of permeability and permittivity.

3.4. Conclusion

In this work we have synthesized cubic, cobalt ferrite and copper ferrite nanoparticles with average particle size 18 nm and 12 nm by sol-gel method using poly acrylic acid as the chelating agent. The extremely fine crystallite size and regular shape of the materials are evident from the FE–SEM images. The average crystallite sizes and the particle sizes are calculated both by XRD and FE-SEM. The results are found to be in good agreement with each other. The saturation magnetization value calculated for $CoFe_2O_4$ is 30 emu/g and for $CuFe_2O_4$ nanoparticles is 15 emu/g, which is also lower than the reported values for the bulk. The average crystallite size of $CoFe_2O_4$ nanoparticles is higher compared to $CuFe_2O_4$ nanoparticles. Very small changes in crystallite size can lead to large changes in coercivity. The increase in magnetization and coercivity of $CoFe_2O_4$ is due to the increase in the crystallite size. The magnetization curves demonstrate that the as-prepared $CuFe_2O_4$ nanoparticles at room temperature tends to be more superparamagnetic compared to $CoFe_2O_4$, as the field is cycled between –10000 and 10000 G. From these results it may be concluded that in the nanocrystalline $CoFe_2O_4$ and $CuFe_2O_4$ samples, the cation distribution stabilizes the cubic form at room temperature and superparamagnetic behavior should be attributed to the extremely fine crystallite size and regular shape of the material.

The complex permeability, complex permittivity and a.c. conductivity in the microwave frequencies are studied using microwave cavity perturbation method. The real part of permittivity shows almost constant values whereas the imaginary part of complex permittivity and the loss tangent decrease slightly with frequency. The a.c. conductivity is found to be varying with

frequency as expected for small polaron hopping. The real and imaginary parts of complex permeabilities and the loss tangents show a decreasing trend. The a.c. conductivity and the Tan δ values of $CoFe_2O_4$ nanoparticles are observed to be high compared to $CuFe_2O_4$ nanoparticles. This can be attributed to the high magnetic moment possessed by $CoFe_2O_4$. The superparamagnetic nature of the $CuFe_2O_4$ and $CoFe_2O_4$ nanoparticles might have affected the experimental values of permeability and permittivity.

3.5. References

1. J. Du, Z. Lu, W. Wu, Z. Li, B. Han, Y. Huang, *Mater. Res. Bull.,* 40 (2005) 928
2. S. Kang, W.J. Harrell, E.D. Nikles, *Nano Lett.,* 2 (2002) 1033
3. D.H. Chen, X.R. He, *Mater. Res. Bull.,* 36 (2001) 1369
4. T. George, S. Joseph, S. Mathew, *J. Metastable and Nanocryst. Mater.,* 23 (2005) 141
5. F.L Buchholz, *Industrial Polymers Handbook-Products, Processes, Applications,* E.S. Wilks (ed), Wiley-VCH, New York, 1 (1986)
6. K.T. Mathew, S.B. Kumar, A. Lonappan, J. Jacob, J. Samuel, T. Xavier, T. Kurian, *Mater. Lett.,* 56 (2002) 248
7. K.T. Mathew, U. Raveendranath, *Sensors Update*, Germany, 7 (1999) 185
8. U. Raveendranath, *Ph.D. thesis,* Mahatma Gandhi University, Kottayam, (1996)
9. R.A. Waldron, *Perturbation Theory of Resonant Cavities, Proc. IEE,* 107C, (1960) 272
10. U. Raveendranath, K.T. Mathew, *Microwave and Opt. Tech. Letters,* 18 (1998) 241

11. R.F. Harrington, *Time Harmonic Electromagnetic fields,* McGraw-Hill, New York, (1961)
12. C. Suryanarayana, M.G. Norton, *X-ray Diffraction a Practical Approach*, Plenum Press, New York, (1998)
13. S. Roy, J. Ghose, *J. Appl. Phys.*, 87(9) (2000) 6226
14. C. Caizer, Stefanescu, *J. Phys. D: Appl. Phys.*, 35 (2002) 3035
15. Q. Chen, Z.J. Zang, *Appl. Phys. Lett.*, 73 (1998) 3156
16. C.P. Bean, J.D. Livingstone, *J. Appl. Phys.*, 30 (1959) 120
17. W.J. Duffin, *Electricity and Magnetism,* McGraw-Hill Book Company, London, (1990)
18. J. Appel, *Solid-State Physics,* F. Seitz, D. Turnbull, H. Ehrenreich (eds), Academic Press, New York, (1968)
19. A.N. Patil, M.G. Patil, K.K. Patankar, V.L. Mathe, R.P. Mahajan, S.A. Patil, *Bull. Mater. Sci.*, 23 (2000) 447
20. D. Adler, Feinleib, *Phys. Rev. B,* 2 (1970) 3112
21. A.J. Baden Fuller, *Ferrites at Microwave Frequencies,* Peter Peregrinus Ltd., London, (1987)
22. S. Krupanicha, *The Physics of Ferrites and Magnetic Oxides Related to Them* (Russian translation) (1st edn.) Mir, Moscow, (1976)
23. G.H. Jonker, *J. Phys. Chem. Solids*, 9 (1959) 105
24. R.K. Wangsness, *Electromagnetic Fields,* John Wiley & Sons, New York, (1979) 25